IEEE Access
Multidisciplinary | Rapid Review | Open Access Journal

Date of publication xxxx 00, 0000, date of current version xxxx 00, 0000.

Digital Object Identifier 10.1109/ACCESS.2017.DOI

Slack and Excessive Loading Avoidance in n-tendon Continuum Robots

MOHSEN MORADI DALVAND[1,2], SAEID NAHAVANDI[1] (Fellow, IEEE) and ROBERT D. HOWE[3] (Fellow, IEEE).

[1]Deakin University, Geelong, Australia, Institute for Intelligent Systems Research and Innovation (IISRI) and Harvard Paulson School of Engineering and Applied Sciences, Cambridge, MA 02138 USA (e-mail: mdalvand@seas.harvard.edu)
[2]Deakin University, Geelong, Australia, Institute for Intelligent Systems Research and Innovation (IISRI) (e-mail: saeid.nahavandi@deakin.edu.au)
[3]Harvard Paulson School of Engineering and Applied Sciences, Cambridge, MA 02138 USA (e-mail: howe@seas.harvard.edu)

Corresponding author: Mohsen Moradi Dalvand (e-mail: mdalvand@seas.harvard.edu).

ABSTRACT In this work, two tendon tension loading distributions (fixed and moving) are designed to prevent undesired slack and excessive loading in tendons of continuum manipulators. For any given beam configuration, the algorithms utilize the proposed loading distributions to find a new beam configuration as well as base displacement to control the orientation or position of the n-tendon continuum robot. The algorithms account for the bending and axial compliance of the manipulator as well as tendon compliance. Numerical results are provided to demonstrate the orientation and position control algorithms under fixed or moving loading distributions. A 6-tendon continuum robot system is employed to experimentally evaluate the effectiveness and accuracy of the proposed control algorithms. Multiple experiments are carried out and results are reported. The results verify the performance of the proposed control algorithms in avoiding slack and excessive loading in tendons and controlling the orientation and position of continuum structures.

INDEX TERMS Continuum Robot, Catheter, Slack Avoidance, Kinematics, Load Analysis, Tendon-driven

I. INTRODUCTION

Continuum robots are inspired by natural continuum structures like elephant trunks [1], octopus arms [2], squid tentacles [3], and snakes [4], [5]. Their continuous structure and inherent compliance enable them to exhibit elastic deformation along their entire length and navigate safely [6]–[11]. In the medical field, catheters and catheter-like instruments are well-known examples of continuum structures that have gained attention in minimally invasive treatments [12], [13].

A direct approach to manipulating a continuum structure is the use of remotely actuated tendons [14], [15]. Tendons can only support tension (negative load) and in compression they go slack because of their low bending stiffness [14], [16]. Actuation of a slacked tendon will first recover the slack before producing tension in the tendon [17]. This latency results in actuator backlash that is one of the key causes of inefficiency and inaccuracy in the controllers of robotic catheters [18]. Slack directly affects the stiffness of the articulating beam and the load distribution among tendons [13]. Although slack may be mitigated by increasing tension loads in all tendons, high tendon load in continuum robots generates less compliance and more friction. Therefore, slack and excessive loading are both undesirable characteristics especially in catheters in which tendon size and materials are constrained by the environment [13], [19].

Methods were introduced to prevent slack based on a redundancy of control actions in redundant rigid-link tendon-driven mechanisms [20]–[24]. A similar approach was employed to prevent slack in redundant tendon-driven continuum robots based on the numerical optimization techniques in a closed-loop control architecture [17], [25], [26]. These studies do not promise reliable control algorithms capable of performing the real-time computations involved in numerical optimization process, especially for higher numbers of tendons. This may cause a drift in Jacobian estimation from the true

estimate and take longer to converge, leading the robot to diverge from the desired path [25]. They also require load cells for online measurement and feedback of the tension loading in tendons [25]. Pretensioning tendons was also utilized in multiple studies [27]–[31]. Excessive pretension causes more friction which leads to faster wear and tear and shorter lifetime [32], [33]. Not enough pretension causes slack and deficiency in control [27].

The main contribution of this study is algorithms to control orientation or tip position of n-tendon continuum robots guaranteeing no slack or excessive loading in tendons. Two loading distributions (fixed and moving) are proposed to minimize the tension loadings to a certain level that causes tension in all tendons (no slack). For any given beam configuration within workspace, the algorithms utilize the proposed loading distributions to find a new beam configuration as well as base displacement to control the orientation or position of the continuum robot.

In the following section, the tension loading model in n-tendon continuum robots used throughout this paper is explained. Slack and excessive loading problems are described and their effects are demonstrated using numerical analysis in Section III. Fixed and moving loading distributions and how they are utilized in orientation and position control algorithms are explained and numerical results are provided in Sections IV and V. Section VI presents details about experimental setup, procedure and results followed by discussion and concluding remarks in Section VIII.

II. LOADING MODEL

Figure 1 shows the schematic description of the articulating beam of a single segment cable-driven continuum robot with n equidistant tendons ($n = 6$ in this case) in an arbitrary beam configuration defined with bending angle (θ), pending plane angle (ϕ), and beam length along its centerline (L). As previously developed [34], the tension load model for i-th tendon in n-tendon continuum robots can be expressed as a function of beam configuration parameters as

$$F_i(\theta,\phi,L) = \frac{EI(k-1)}{nL_0R_a}\theta\cos(\phi-\alpha_i) - (L_0-L)\frac{EA}{nL_0} \quad i=1,\dots,n \tag{1}$$

where i is tendon number ($i = 1,\dots,n$), E, I and A are the Young's modulus, area moment of

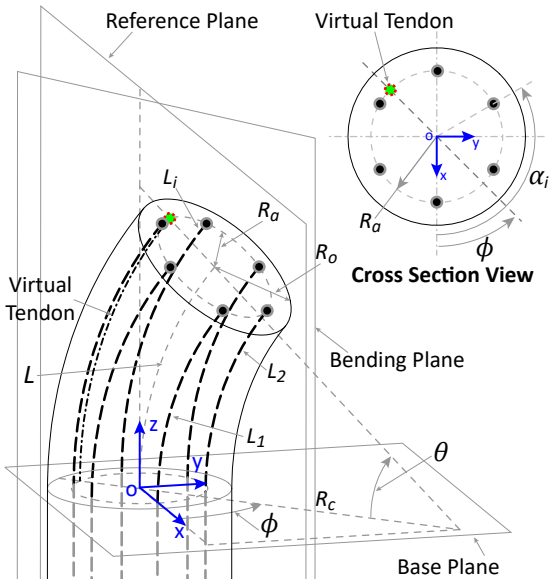

FIGURE 1: Schematic description of the articulating beam of a tendon-driven catheter with n equidistant tendons ($n = 6$ in this description) at a beam configuration ($[\theta, \phi, L]$)

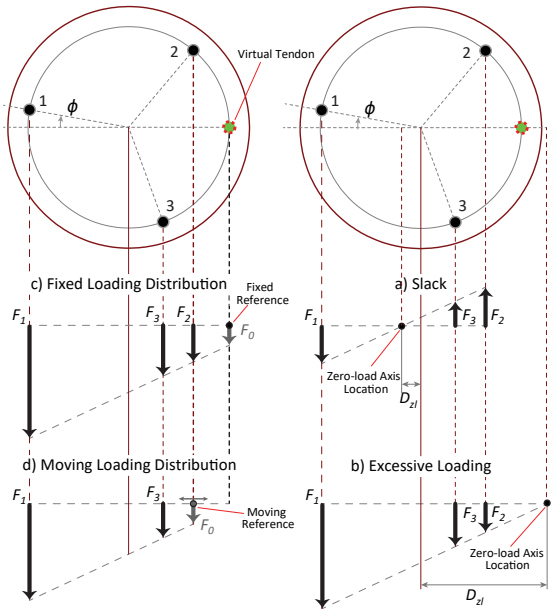

FIGURE 2: Schematic presentation of different loading distributions with (a) slack (b) and excessive loading as well as (c) fixed and (d) moving loading distribution in a n-tendon continuum robot ($n = 3$ in this description)

inertia, and cross section area of the beam, R_a and α_i are radial and angular location of tendons, L_0 is the initial length of the continuum structure, and k is representative of number of degrees of freedom (DOF) of the continuum robot and is defined as

$$k = \begin{cases} n & \text{if} \quad n = 1, 2 \\ 3 & \text{if} \quad n \geq 3 \end{cases} \tag{2}$$

The angular location of i-th tendon (α_i) of n equidistant tendons can be represented by $^{2\pi}/_{n}(i-1)$. In Figure 1, a *virtual* tendon is defined that is located at the back of the continuum structure on the bending plane at the distance R_a from the centerline.

Figure 2 schematically presents different loading distributions in a n-tendon continuum robot ($n = 3$ in this example). As demonstrated in this figure, applying actuator displacements obtained from the inverse kinematics solution for a given configuration results in unique set of tendons tensions in a continuum robot that are linearly distributed among the tendons [34]. The conceptual axis on the cross section of the continuum structure, perpendicular to the bending plane, with zero tension in tendons lying on it is called zero-load axis. The location of this axis from the centerline of the continuum structure is denoted by D_{zl} and can be derived as [34]

$$D_{zl} = \frac{AR_a^2}{2I\theta}(L_0 - L) \tag{3}$$

This axis is different from the neutral axis with zero displacement in tendons lying on it. The location of the neutral axis from the centerline of the continuum structure can be derived as $D_{zd} = {}^{(L_0-L)}/_{\theta}$.

In order to illustrate the behavior of the tendon loading for different beam configurations and demonstrate the effects of slack and excessive loadings in tendons, numerical simulations are performed and the results are provided in the following section. Similar simulations are also utilized to evaluate the performance of the developed control algorithms for slack and excessive loading avoidance and the results are also described in the following sections.

III. SLACK AND EXCESSIVE LOADING

Figure 3 presents results for the numerical simulations for the estimated tendon tension loads in a 6-tendon continuum robot at different sets of beam configurations. The mechanical specification

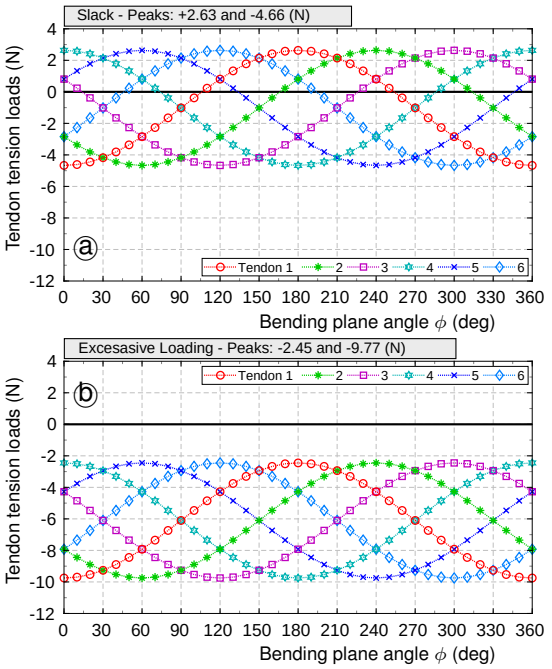

FIGURE 3: Numerical simulation results for the tendon tension loads in a 6-tendon continuum robot at the beam configurations (a) $[\theta, \phi, L_{SS}]$ and (b) $[\theta, \phi, L_E]$. Parameters are listed in Tables 1 and 2.

TABLE 1
MECHANICAL SPECIFICATION OF THE CONTINUUM ROBOT

Mechanical Parameter	Value
Number of tendons (n)	6
Beam Young's modulus (E)	5.9 MPa
Radial tendon location (R_a)	3.5 mm
Beam radius (R_o)	6 mm
Beam initial length (L_0)	160 mm
Tendon Young's modulus (E_t)	48.9 GPa
Tendon radius (R_t)	0.23 mm
Tendon initial length (L_{t_0})	435.54 mm

of the continuum structure used in the simulation are chosen identical to those from the experimental setup (Table 1). The beam configurations $[\theta, \phi, L_{SS}]$ and $[\theta, \phi, L_E]$ (Table 2) served as inputs to estimate tendon tension loads using Equation (1) for the first and second simulations, respectively. These configurations are selected to respectively demonstrate slack (in some of the tendons) and excessive loading in tendons as presented in Figures 2a and 2b. Table 3 includes parametric results of the numerical analysis.

As shown in Figure 3a, in every configuration, there are tendons with positive tension values (peak

TABLE 2
BEAM CONFIGURATIONS USED IN NUMERICAL ANALYSIS AND EXPERIMENTS

Beam configuration parameter	Value
Bending angle (θ)	40 deg
Bending plane angle (ϕ)	[0, 10, 20,..., 360] deg
Length - Some slack (L_{SS})	159 mm
Length - Excessive loading (L_E)	154 mm
Length - All slack (L_{AS})	175 mm

values of +2.63 and -4.66 N). This means that in order to reach these configurations, some of the tendons must act like a solid rod and push (positive loading as shown in Figure 2a). However, tendons can only support tension (negative load) and in compression they tend to buckle (go slack) because of their low bending stiffness. Actuation of a slacked tendon results in inefficiency and inaccuracy in the control of robotic catheters [13], [34].

It should be noted that slack may be produced in tendons even when the beam structure is under compression. For example, there is 1 mm compression across all beam configurations in the first simulation. This is because of the zero-load axis located inside the beam structure; $D_{zl} < R_a$ (Figure 2a and Table 3, #1). This generates different loading directions in tendons located on opposite sides of this axis [34] and results in the summation of the tension loads to be as low as -6.10 N (Table 3, #1).

The second simulation is an example of excessive loading in tendons (Figures 2b and 3b). Although θ and ϕ used in both simulations have similar values, the beam structure in the second simulation is under 5 mm additional compression which causes more loading in tendons (peak values of -2.45 and -9.77 N as listed in Table 3, #2). In this simulation, the zero-load axis is located outside of the beam structure; $D_{zl} > R_a$ (Figure 2b and Table 3, #2). This generates similar loading directions in all tendons. As shown in Figure 3b, there is no slack in any of the tendons across all configurations; however, tendons are always under tension even at their minimum contribution (Figure 2b). This results in the large value of -36.60 N for the summation of tension loads. High tendon tension in continuum robots generates less compliance and more friction [29], [33].

Therefore, slack and excessive loading are both undesirable characteristics especially in catheters in which tendon size and materials are constrained by the environment [17]. Given the above examples, the question is how can slack in continuum robots be avoided without producing excessive loading in tendons? The proposed solution is to determine, based on fixed and moving loading distributions, new beam configuration as well as base displacement to satisfy no-slack and excessive loading conditions for orientation and position controls.

IV. FIXED LOADING DISTRIBUTION

To prevent slack in a continuum robot, target beam configurations requiring tendon tensions larger than zero should be prevented. As shown in Figure 2c, this can be achieved by pushing the location of the zero-load axis at or behind the virtual tendon ($D_{zl} \geq R_a$). The bigger $|D_{zl} - R_a|$, the more tension loading in tendons. To minimize the loading distribution and still have no slack in any of the tendons, the zero-load axis can be located right at the location of the virtual tendon ($D_{zl} = R_a$). In order to also control the stiffness of the continuum manipulator, as shown in Figure 2c, the tension loading F_0 (instead of zero) is considered at the location of the virtual tendon (see Discussion). In this approach, the location of the zero-load axis is independent of beam configuration and same minimum F_0 loading condition can be satisfied for all configurations. This results in a loading distribution with fixed zero-load axis location that is referred to as the *fixed loading distribution* in this paper (Figure 2c).

The location of the bending plane at which the peak tension loads in the i-th tendon happen may be determined by differentiating F_i from Equation (1) with respect to ϕ ($dF_i/d\phi = 0$) as

$$\phi_{i_f} = \alpha_i + m\pi \quad \begin{cases} i = 1, \ldots, n \\ m \in \mathbb{N} \end{cases} \tag{4}$$

As implied from this equation, the peak tension loads in each tendon happen when it lies on the bending plane. Even and odd values of parameter m result in the angular location of the maximum and minimum magnitude of the tension loadings in the i-th tendon. Substituting odd values of m in Equation 4 determines the bending plane at which the i-th tendon is on the virtual tendon. To satisfy the minimum tension loading F_0 in the i-th tendon at the bending plane angle of ϕ_{i_f}, Equation (4) can be substituted in Equation (1) as

$$F_i(\theta, \phi_{i_f}, L) = F_0 \quad \begin{cases} i = 1, \ldots, n \\ m = 1 \end{cases} \tag{5}$$

TABLE 3
RESULTS OF THE NUMERICAL SIMULATIONS

Simulation	Given config.	Target config.	Tension peaks (N)	D_{zl} (mm)	D_{zd} (mm)	$\Delta Z_{f(m)p}$ mm	$\sum_{i=1}^{n} F_i$ (N)
#1 - Some slack	$[\theta, \phi, L_{SS}]$	$[\theta, \phi, L_{SS}]$	$[-4.66, +2.63]$	+0.97	+1.43	0.00	-6.10
#2 - Excessive loading	$[\theta, \phi, L_E]$	$[\theta, \phi, L_E]$	$[-9.77, -2.45]$	+5.84	+8.59	0.00	-36.60
#3 - Fixed - Orientation	$[\theta, \phi, L_{SS}]$	$[\theta, \phi, L_{fo}]$	$[-7.30, 0.00]$	+3.50	+5.14	0.00	-21.90
#4 - Fixed - Position	$[\theta, \phi, L_{SS}]$	$[\theta_{fp}, \phi, L_{fp}]$	$[-7.43, 0.00]$	+3.50	+5.14	+2.89	-22.30
#5 - Fixed - Position	$[\theta, \phi, L_E]$	$[\theta_{fp}, \phi, L_{fp}]$	$[-7.17, 0.00]$	+3.50	+5.14	-2.68	-21.52
#6 - Moving - Orientation	$[\theta, \phi, L_{SS}]$	$[\theta, \phi, L_{mo}]$	$[-7.30, 0.00]$	[+3.03 to +3.50]	[+4.45 to +5.14]	0.00	[-21.90 to -18.97]
#7 - Moving - Position	$[\theta, \phi, L_{SS}]$	$[\theta_{mp}, \phi, L_{mp}]$	$[-7.43, 0.00]$	[+3.03 to +3.50]	[+4.45 to +5.14]	[+2.35 to +2.89]	[-22.30 to -19.20]
#8 - Moving - Position	$[\theta, \phi, L_E]$	$[\theta_{mp}, \phi, L_{mp}]$	$[-7.17, 0.00]$	[+3.03 to +3.50]	[+4.45 to +5.14]	[-3.21 to -2.68]	[-21.52 to -18.57]

By solving this equation with respect to L, the new length of the continuum structure (L_f) guaranteeing minimum tension loading F_0 is derived as a function of θ as

$$L_f(\theta) = C_1 - C_2\theta \quad k \geq 2 \tag{6}$$

where constant parameters C_1 and C_2 are

$$C_1 = L_0\left(\frac{nF_0}{AE} + 1\right)$$
$$C_2 = \frac{I(k-1)}{AR_a}$$

The constraint $k \geq 2$ in this equation is because slack is meaningless in case of single tendon robot. It is worth noting that L_f is independent of parameters i, L, and ϕ and is a function of only θ. In the following sections, control algorithms are developed based on the fixed loading distribution in order to enable orientation and position control of continuum robot while satisfying minimum F_0 tension constraint (no slack).

A. ORIENTATION CONTROL

Figure 4 illustrates the beam structure at different configurations and under various control scenarios. The beam structure illustrated with solid line represents a target beam configuration in which tendons are under excessive loading or slack. In some applications, the orientation of the tip of the continuum robot or catheter is more important than its position, e.g. pointing an ultrasound imaging catheter [35]. In order to manipulate a continuum structure to the given bending angle θ under the fixed loading distribution, Equation (6) may be used to find the length of the continuum structure L_{fo} satisfying minimum F_0 loading in tendons as

$$L_{fo} = L_f(\theta) \quad k \geq 2 \tag{7}$$

The dashed line in Figure 4 illustrates the beam structure under orientation control with similar θ as of the solid line. Based on the Equation (7), for orientation control under fixed loading distribution, only parameters θ and ϕ are required and the algorithm determines the maximum possible length of the continuum structure (L_{fo}) at which there is minimum F_0 loading in tendons (no slack or excessive loading). Substituting Equation (7) into the Equation (1), the tendon tensions for orientation control of a n-tendon continuum robot under fixed loading distribution is derived as

$$F_{i_{fo}}(\theta, \phi) = F_0 - \frac{EI(k-1)}{nL_0R_a}\theta \times \left(\cos(\phi - \alpha_i) + 1\right) \quad \begin{cases} i = 1, \ldots, n \\ k \geq 2 \end{cases} \tag{8}$$

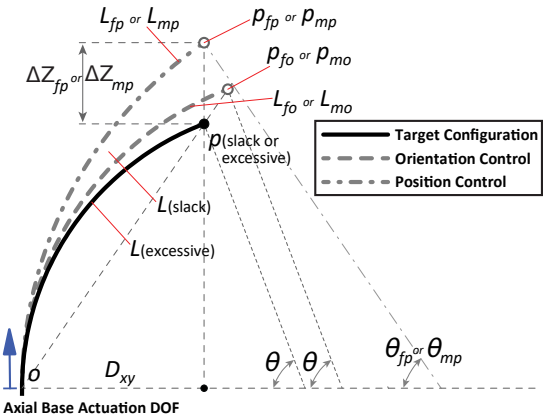

FIGURE 4: Schematic description the beam structure at different configurations and under various control scenarios (*solid lines*: target configuration causing slack or excessive loading in tendons, *dashed line*: orientation control under fixed or moving loading distribution, *dash-dot lines*: position control under fixed or moving loading distribution for slack and excessive loading cases)

This article has been accepted for publication in a future issue of this journal, but has not been fully edited. Content may change prior to final publication. Citation information: DOI 10.1109/ACCESS.2020.3012036, IEEE Access

A characteristic feature of fixed loading distribution is the minimum F_0 loading in the virtual tendon (Figure 2c). This can be demonstrated using Equation (8) by calculating the tension load in the 4-th tendon ($F_{4_{fo}}$) of a 6-tendon robot at $\phi = 0$ ($\phi - \alpha_4 = -\pi$) which makes it lay on the virtual tendon ($F_{4_{fo}} = F_0$). Using Equation (8), the summation of the tension loads of all tendons for orientation control of a continuum robot under fixed loading distribution for any given configuration $[\theta, \phi, L]$ can be derived as a function of θ as

$$\sum_{i=1}^{n} F_{i_{fo}} = nF_0 - \frac{EI(k-1)}{L_0 R_a}\theta \quad k \geq 2 \tag{9}$$

Based on the beam configuration and tendon tension, tendon displacements ΔL_i, tendon stretches δ_i, and actuator displacements (ΔL_{a_i}) can be determined using

$$\Delta L_i = (L_0 - L) + R_a\theta\cos(\alpha_i - \phi) \quad i = 1, ..., n \tag{10}$$

$$\delta_i = \frac{F_i L_{t_0}}{E_t A_t} \quad i = 1, \ldots, n \tag{11}$$

$$\Delta L_{a_i} = \Delta L_i + \delta_i \quad i = 1, \ldots, n \tag{12}$$

To control orientation of a continuum robot under fixed loading distribution, target θ and ϕ are used in Equation (7) to determine the desired length of the continuum structure (L_{fo}). The new beam configuration $[\theta, \phi, L_{fo}]$ can then be used to determine ΔL_{a_i} to reach orientation θ and satisfy no-slack and minimum F_0 loading conditions (Algorithm 1).

To demonstrate the effectiveness of the orientation control algorithm under fixed loading distribution in satisfying F_0 loading constraint (no slack), the numerical simulation process for the beam configurations $[\theta, \phi, L_{SS}]$ and $[\theta, \phi, L_E]$ are repeated based on this control algorithm. The minimum loading is set to zero ($F_0 = 0$). The results are presented in Figure 5a. The orientation control algorithm is independent of the given L as it determines the required beam length (L_{fo}) to satisfy the desired conditions. Therefore, the results for both configurations $[\theta, \phi, L_{SS}]$ and $[\theta, \phi, L_E]$ are similar.

As shown in Figure 5a compared to Figure 3, the peak values are changed to 0 and -7.3 N (Table 3, #3) which means that tendons are never under positive tension for any configuration. Tendon tension summation (Equation (9)) is a function of only θ that results in a constant value of -21.90 N in this simulation. As expected, this value is decreased significantly compared to the summation of tensions in the simulation for the excessive loading in tendons (Figure 3b and Table 3, #3). On the other hand, there is no excessive loading in tendons as their tensions reach the minimum absolute values of zero ($F_0 = 0$ in this case) when they meet the virtual tendon (Figure 2c). In all other configurations, the absolute values of the tensions in all tendons are always bigger than $|F_0|$, e.g. at $\phi = 90°$ in Figure 5a. In other words, in case of fixed loading distribution, the magnitude of the tensions in all tendons are always greater than F_0 except that of the tendon laid on the virtual tendon with tension equal to F_0. This is another characteristic feature of the fixed loading distribution that exists for both orientation and position control algorithms.

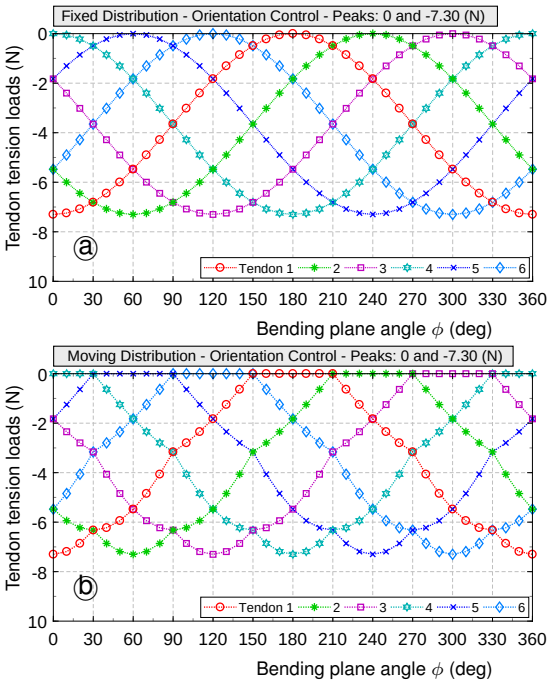

FIGURE 5: Simulation examples for the estimated tendon tension loads in a 6-tendon continuum robot at the beam configuration $[\theta, \phi, L_{SS}]$ for orientation control under (a) fixed and (b) moving loading distributions. Parameters are defined in Table 2.

B. POSITION CONTROL

To control the tip position of a continuum robot and satisfy no-slack and minimum F_0 loading conditions, the fixed loading distribution can be utilized in combination with an axial actuated DOF of the base of the continuum structure, i.e. insertion/retraction

Algorithm 1: Orientation control algorithm under fixed (or moving) loading distribution

input : Bending angle (θ), bending plane angle (ϕ), minimum loading (F_0), and geometry and mechanical properties of beam and tendons ($[p]$)

output: Tendon actuator displacements $[\Delta L_{a_i}]$

Algorithm `ControlOrientation`(θ, ϕ, F_0, $[p]$)

Determine L_{fo} using Equation (7) (or L_{mo} using Equation (21));
Determine tendon displacements $[\Delta L_i]$ using Equation (10) ;
Determine tendon tensions $[F_{i_{fo}}]$ using Equation (8) (or $[F_{i_{mo}}]$ using Equation (22));
Determine tendon stretches $[\delta_i]$ based on the tendon tensions $[F_{i_{fo}}]$ (or $[F_{i_{mo}}]$) using Equation (11);
Determine tendon actuator displacements $[\Delta L_{a_i}]$ using Equation (12);
return $[\Delta L_{a_i}]$;

of the catheter shaft. The dash-dot line in Figure 4 illustrates the beam structure under position control. As shown in this figure, a continuum robot commanded to $[x,\ y,\ z]$ coordinates (point p in the figure) can instead be manipulated to a new coordinates $[x, y, z_{fp}]$ (point p_{fp} in the figure) while the axial actuated DOF of the base compensates for z and z_{fp} differences (ΔZ_{fp}). To meet minimum F_0 loading condition as well as x and y coordinates condition, two constraints are defined. The first constraint is to guarantee minimum F_0 loading in tendons (no slack) which is defined based on the Equation (6) as

$$L_{fp} = R_{fp}\theta_{fp} = C_1 - C_2\theta_{fp} \quad k \geq 2 \tag{13}$$

where L_{fp} in the new length of the continuum structure that can be represented by multiplying the radius of the beam structure (R_{fp}) by the new beam bending angle (θ_{fp}). L_{fp} and θ_{fp} are the unknown beam parameters satisfying the desired conditions. As shown in Figure 4, the tip position of the dash-dot line (point p_{fp}) have similar x and y coordinates as of those of the solid lines (point p). Therefore, both tip points p and p_{fp} (Figure 4) projected upon xy plane should be equidistant from the origin. The second constraint is defined as

$$R_{fp} = \frac{1-\cos(\theta)}{1-\cos(\theta_{fp})} \times \frac{L}{\theta} \tag{14}$$

To find the two unknown variables R_{fp} and θ_{fp}, Equation (14) is substituted into Equation (13):

$$\Big(C_2 + \frac{1-\cos(\theta)}{1-\cos(\theta_{fp})} \times \frac{L}{\theta}\Big)\theta_{fp} = C_1 \tag{15}$$

By finding θ_{fp} from this equation and substituting it back into Equation (14) and then in Equation (13), both configuration variables L_{fp} and θ_{fp} are determined. The required base displacement to compensate for the changes in z coordinates of points p and p_{fp} (Figure 4) can be derived as

$$\Delta Z_{fp} = \frac{L}{\theta}\Big(\sin(\theta) - \frac{1-\cos(\theta)}{1-\cos(\theta_{fp})} \times \sin(\theta_{fp})\Big) \tag{16}$$

As described in Algorithm 2, to manipulate a continuum robot to a given tip position $[x,\ y,\ z]$ (corresponding to the configuration $[\theta, \phi, L]$) and also satisfy no-slack condition under fixed loading distribution, the robot can be commanded to the beam configuration $[\theta_{fp}, \phi, L_{fp}]$ while the displacement ΔZ_{fp} is simultaneously commanded to the axial base DOF. Numerical simulations are performed for the configurations $[\theta, \phi, L_{SS}]$ and $[\theta, \phi, L_E]$ and $F_0 = 0$ based on the position control algorithm under fixed loading distribution. The results have similar patterns to those presented in Figure 5a but different peak values (Table 3, #4 and #5). As implied from numerical results, position control algorithm satisfies no-slack condition. However, it requires extra DOF of the base to compensate for ΔZ_{fp}.

V. MOVING LOADING DISTRIBUTION

To prevent slack in a continuum robot, zero-load axis can be pushed at or behind the location of the virtual tendon at the back of the continuum structure ($D_{zl} \geq R_a$). In case of fixed loading distribution, the minimum loading in tendons guaranteeing no slack in tendons happens when the zero-load axis is located right at the location of the virtual tendon ($D_{zl} = R_a$). The magnitude of this loading distribution can be further decreased whenever the bending plane does not coincide with a tendon location (Figure 2). To minimize the loading distribution

Algorithm 2: Position control algorithm under fixed (or moving) loading distribution

input : Tip position ($[x, y, z]$), minimum loading (F_0), and geometry and mechanical properties of beam and tendons ($[p]$)

output: Tendon actuator displacements $[\Delta L_{a_i}]$, base actuator displacement ΔZ_{fp} (or ΔZ_{mp})

Algorithm `ControlPosition`($[x, y, z]$, F_0, $[p]$)

Determine beam configuration parameters $[\theta, \phi, L]$ of the tip position $[x, y, z]$ [36];
Determine θ_{fp} using Equation (15) (or θ_{mp} using Equation (28));
Determine L_{fp} using Equation (13) (or L_{mp} using Equation (26));
Determine tendon displacements $[\Delta L_i]$ using Equation (10) ;
Determine tendon tensions $[F_i]$ using Equation (1);
Determine tendon stretches $[\delta_i]$ Equation (11);
Determine tendon actuator displacements $[\Delta L_{a_i}]$ using Equation (12);
Determine base actuator displacement ΔZ_{fp} using Equation (16) (or ΔZ_{mp});
return $[\Delta L_{a_i}]$, ΔZ_{fp} (or ΔZ_{mp});

magnitude to the lowest possible value and still satisfy the no-slack condition, the zero-load axis can be located at the location of the farthest tendon at the back of the continuum structure.

To avoid slack and unnecessary loading in tendons under moving loading distribution and also be able to potentially adjust stiffness in continuum structure, the location of the zero-load axis can be moved behind the farthest tendon at the back of the continuum structure such that there is a minimum tension loading of F_0 in the farthest tendon at the back. An illustration of this loading distribution is presented in Figure 2d. As ϕ changes, the location of the farthest tendon and consequently the zero-load axis location and the loading distribution magnitude changes. This results in a loading distribution that is referred to as the *moving loading distribution* in this paper. Equation (1) can be used to equate tension in the farthest tendon at the back of the continuum structure (tendon i_m) to F_0 as

$$F_i(\theta, \phi, L_c) = F_0 \quad i = i_m \tag{17}$$

where i_m is determined as

$$i_m = \underset{\{i:i=1,\dots,n\}}{\arg\min} \left(R_a \cos\left(\phi - \alpha_i\right) \right)$$

Using Equation (17), the new length of continuum structure satisfying minimum F_0 loading condition is derived as

$$L_m(\theta) = C_1 + C_2\theta \cos\left(\phi - \alpha_{i_m}\right) \tag{18}$$

The differences between L_m and L_f (Equation 6) is

$$L_m - L_f \begin{cases} = 0, & \text{if } \alpha_{i_m} - \phi = \pi \\ > 0, & \text{otherwise} \end{cases} \tag{19}$$

As implied, the length of the beam structure under moving loading distribution is always bigger than its length under fixed loading distribution, unless the i_m-th tendon is laid on the bending plane ($\alpha_{i_m} - \phi = \pi$). This is because $(\alpha_{i_m} - \phi)$ is always larger than $\pi/2$ which means that L_f and L_m only equate when the later has its minimum value

$$L_f = \min(L_m) \tag{20}$$

This produces less compression in the continuum structure and consequently less tension in tendons. Both orientation and tip position of a continuum robot can be controlled under moving loading distribution that are explained in the following sections.

A. ORIENTATION CONTROL

To control the pointing angle of a continuum robot under moving loading distribution, Equation (18) may be used to find the length of the continuum structure (L_{mo} in Figure 4) satisfying the minimum F_0 loading condition as

$$L_{mo} = L_m(\theta) \quad k \geq 2 \tag{21}$$

Similar to orientation control under fixed loading distribution, to control orientation angle under moving loading distribution, parameters θ and ϕ are needed for the algorithm to obtain the maximum length of the continuum structure (L_{mo}) satisfying

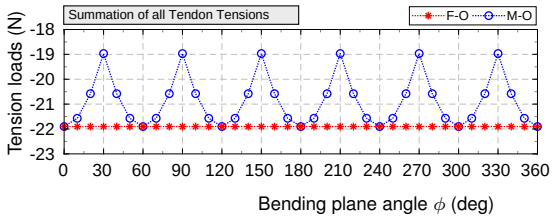

FIGURE 6: Summation of the tension loads in all tendons calculated in the simulation for orientation control under both fixed and moving loading distributions with respect to the bending plane angle ϕ

F_0 loading condition (Algorithm 1). Substituting Equation (21) into the Equation (1), the required tendon tensions for orientation control of a n-tendon continuum robot under moving loading distribution is

$$F_{i_{mo}}(\theta,\phi) = F_0 - \frac{EI(k-1)}{nL_0R_a}\theta\times \Big(\cos(\phi-\alpha_i)-\cos(\phi-\alpha_{i_m})\Big) \quad \begin{cases} i=1,\dots,n \\ k\geq 2 \end{cases} \tag{22}$$

The behavior of the orientation control algorithm under moving loading distribution is studied using the numerical simulation for similar beam configurations and F_0 as in previous simulations. The results are presented in Figure 5b. This orientation control algorithm is also independent of the given L and, therefore, for both given L_{SS} and L_E, the results are similar. The peak values of the tendon tensions in this simulation (Table 3, #6) are identical to those of the orientation control under fixed loading distribution (Table 3, #3 and Figure 5b) which demonstrates the effectiveness of this algorithm in avoiding slack and excessive loading the tendons.

The summation of the tension loadings in all tendons for orientation control of a continuum robot under moving loading distribution can be derived from (Equation 22) as

$$\sum_{i=1}^{n} F_{i_{mo}} = nF_0 + \frac{EI(k-1)}{L_0R_a}\theta\times \cos(\phi-\alpha_{i_m}) \quad k\geq 2 \tag{23}$$

Comparing this equation with Equation (9) results in

$$\Big|\sum_{i=1}^{n} F_{i_{mo}}\Big| - \Big|\sum_{i=1}^{n} F_{i_{fo}}\Big| \begin{cases} =0, & \text{if } \alpha_{i_m}-\phi=\pi \\ <0, & \text{otherwise} \end{cases} \tag{24}$$

which means that manipulating a continuum robot under moving loading distribution always produces less tendon tensions than those produced under fixed loading distribution unless the i_m-th tendon is laid on the bending plane ($\alpha_{i_m}-\phi=\pi$). This can be expressed as

$$\Big|\sum_{i=1}^{n} F_{i_{fo}}\Big| = \max\Big(\Big|\sum_{i=1}^{n} F_{i_{mo}}\Big|\Big) \tag{25}$$

Figure 6 shows the simulation results for summation of the tension loads for orientation control under fixed and moving average distributions with respect to ϕ. As shown in this figure and also implied from (Equation 23), unlike the summation of tensions in orientation control under fixed loading distribution (Equation (9)) that is a function of only θ, this summation under moving distribution is a function of both θ and ϕ. Therefore, it has variable values ranging from -18.97 N to -21.9 N (Table 3, #6). The results verify Equation (25). The moving loading distribution also causes movements in both locations of zero-load and neutral axes (Table 3, #6).

There is no excessive loading in tendons as their tensions reach the minimum absolute values of zero ($F_0 = 0$ in this case) when they meet the virtual tendon (Figure 2d). A characteristic feature of the moving loading distribution, as shown in Figure 5b, is that in every beam configurations one of the tendons has the minimum F_0 tension loading. This is a key difference between the fixed and moving loading distributions as in fixed loading distribution the tension in one of the tendons is F_0 only when the tendon is laid on the bending plane. Similar to fixed loading distribution, this feature exists in both orientation and position control under moving loading distribution.

B. POSITION CONTROL

It is also possible to control the tip position of a continuum robot under moving loading distribution to avoid slack and excessive loading in tendons. However, similar to position control under fixed loading distribution, an axial displacement of the base of the continuum structure is needed to reach the target tip position. Two constraints are defined

to satisfy no slack and excessive loading as well as x and y coordinates conditions. The first constraint is to have minimum F_0 loading on the i_m-th tendon which is, based on the Equation (18), defined as

$$L_{mp} = R_{mp}\theta_{mp} = C_1 + C_2\theta_{mp}\cos\left(\phi - \alpha_{i_m}\right) \tag{26}$$

where R_{mp}, θ_{mp}, and L_{mp} are the new radius, bending angle, and length of the continuum structure satisfying the desired conditions represented by the dash-dot line in Figure 4. The second constraint guaranteeing similar x and y coordinates for both tip points p and p_{mp} is defined as

$$R_{mp} = \frac{1-\cos(\theta)}{1-\cos(\theta_{mp})} \times \frac{L}{\theta} \tag{27}$$

Substituting Equation (27) into Equation (26) leads to a single-variable equation in θ_{mp}

$$\frac{C_1}{\theta_{mp}} + C_2\cos(\phi - \alpha_{i_m}) = \frac{1-\cos(\theta)}{1-\cos(\theta_{mp})} \times \frac{L}{\theta} \tag{28}$$

Opposed to θ_{fp} determined from Equation (15) which is a function of only θ, θ_{mp} derived from Equation (28) is a function of θ, ϕ, and α_{i_m}. This introduces dependency to ϕ and α_{i_m} in parameters L_{mp} and consequently ΔZ_{mp} and $F_{i_{mp}}$. By finding θ_{mp} from Equation (28) and substituting it back into Equation (27) and then in Equation (26), configuration variables L_{mp} and θ_{mp} are determined. Similar to position control under moving loading distribution, the required base displacement to compensate for ΔZ_{mp} can be derived using Equation (16) based on θ_{mp}.

As described in Algorithm 2, to manipulate a continuum robot to the beam configuration [θ, ϕ, L] corresponding to the given tip position [x, y, z] under moving loading distribution, the robot and base DOF should be commanded to the beam configuration [θ_{mp}, ϕ, L_{mp}] and ΔZ_{mp}, respectively. This moves the tip of the continuum structure to [x, y, z] coordinates and satisfy no-slack and minimum F_0 loading conditions.

The numerical simulations for similar beam configurations and $F_0 = 0$ for position control of a 6-tendon continuum robot under moving loading distribution results in similar tendon tension pattern as shown in Figure 5b, but with different peak values (Table 3, #7 and #8). As expected, these peak values are still identical with those of the position control under fixed loading distribution. The results verify the expected dependency of ΔZ_{mp} and $F_{i_{mp}}$ to ϕ and α_{i_m} parameters as well as their relations with ΔZ_{fp} and $F_{i_{fp}}$.

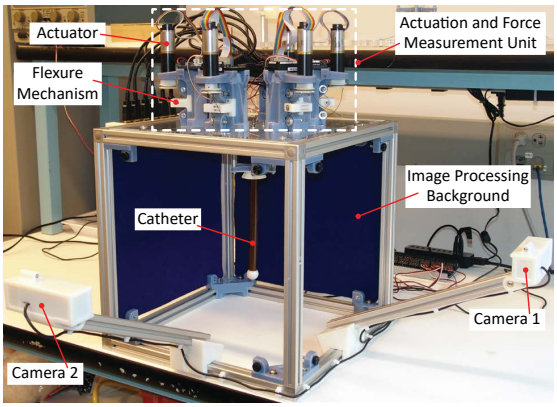

FIGURE 7: The developed modular continuum robotic system capable of manipulating robots with up to 6 tendons integrated with a real-time vision-based 3D reconstruction system [34]

VI. EXPERIMENTS

A. EXPERIMENTAL SETUP

The 6-tendon robotic catheter system, shown in Figure 7, is employed to experimentally evaluate the control algorithms and validate simulation results. The system is integrated with a real-time vision-based shape sensing system that enables the 3D reconstruction of the catheter tube at the rate of 200 Hz with accuracy of ± 0.6 mm and ± 0.5 deg for the linear and angular parameters, respectively [37]. DC geared motors (Model EC-max 22, Maxon Motors Inc., 6072 Sachseln, Switzerland) are utilized for the actuation of the tendons. The base of this robotic system is fixed and not actuated. Load-cells (Model FC22, Phidgets Inc., Calgary, Canada) are incorporated into the actuation modules using a flexure mechanism to measure the tension loads in tendons.

Mechanical parameters of the continuum structure and tendons are listed in Table 1 which are similar to those used in the numerical simulations. Although these parameters are readily available for the prototype in the experimental setup, they need to be either measured or obtained from manufacturer for off-the-shelf continuum robots and catheters. Tendons used in this setup are Spectra microfilament braided lines (Spectra, PowerPro Inc., Irvine, CA, United States). To decrease the friction between the tendon and pulleys, low-friction pulleys with ball bearing are employed in the system. The 6-lumen catheter was molded of urethane rubber (PMC 780, Smooth-On Inc., Macungie, PA, United States). The Young's modulus of the tubes and tendons are measured using an Instron 5566 universal testing machine. Tendons are passed through the lumens and

knotted to the actuator spools from one end and to a cap part from the other end at termination point at distal end of the catheter. The system was operated by a PC with Intel Core i7 processors running at 3.00 GHz with 16 Gb of memory.

B. EXPERIMENT PROCEDURE AND RESULTS

To evaluate the effectiveness of the proposed methods, the cases presented in Figure 3, namely beam configurations $[\theta, \phi, L_{SS}]$ and $[\theta, \phi, L_E]$ respectively causing slack and excessive loading using inverse kinematics solution, as well as the beam configurations modified by the proposed algorithms to avoid slack and excessive loadings are experimentally examined and the results are presented here. F_0 is considered zero in experiments. Before commanding the robot to a configuration, the catheter was commanded to its home configuration (at rest in vertical position with zero tension in tendons) as shown in Figure 7.

Figure 8 presents the experimental results for the beam configurations of [θ, ϕ, L_{SS}] and [θ, ϕ, L_E] causing slack and excessive loading in tendons, respectively. As implied from Figure 8a (peak values of 0 and -5.34 N), at most of the configurations, tendons have zero tension loads which is an indication of slacked tendon. Slacked tendons do not produce any load, therefore, slacked tension loads measured by load-cells at these configurations are zero. Results shown in Figure 8b presents excessive loadings in tendons ranging from -2.56 to -10.96 N. Experimental results are in good confirmation with simulation results (Figure 3) in terms of trend and magnitude for both cases of slack and excessive loading (Table 3). It is worth noting that the tension loads obtained from all experiments have higher magnitudes than corresponding loads obtained from numerical simulations. This correlation that exists across all experiments may be due to friction, nonlinearity, and viscoelasticity in the materials [32], [33].

Experimental results for orientation control algorithm under fixed loading distribution for beam configurations $[\theta, \phi, L_{SS}]$ are presented in Figure 9a. Figures 9b and 9c display the tendon tensions measured in experiments for the position control algorithm under fixed loading distribution for beam configurations $[\theta, \phi, L_{SS}]$ and $[\theta, \phi, L_E]$, respectively. Figure 10 presents the experimental results for orientation and position control algorithms under moving loading distribution based on the beam configurations $[\theta, \phi, L_{SS}]$ and $[\theta, \phi, L_E]$. Both orientation and position control algorithms under fixed

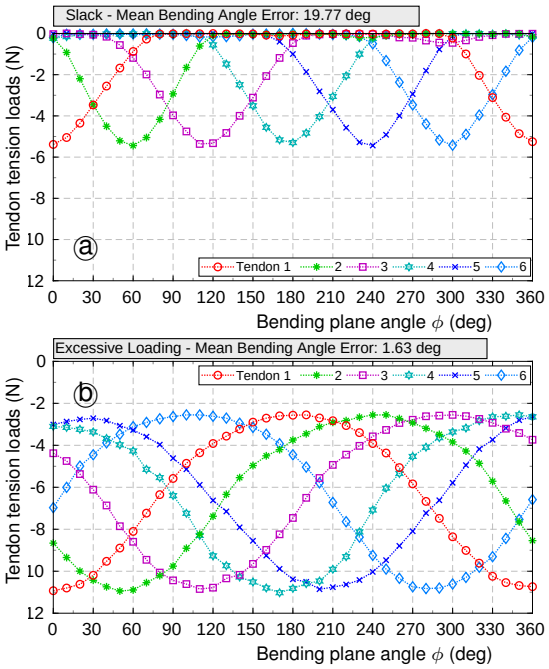

FIGURE 8: Experimental results for the tendon tension loads in a 6-tendon continuum robot for the beam configurations (a) $[\theta, \phi, L_{SS}]$ causing mean bending error of 19.77 deg and $[\theta, \phi, L_E]$ (b) causing mean bending angle error of 1.63 deg

and moving loading distributions satisfy no-slack and minimum F_0 ($F_0 = 0$ in experiments) loading conditions. They also match the simulation results listed in Figure 5 in terms of peak values and loading distributions.

Figures 11a and 11b present errors in the bending angles measured in experiments with respect to the desired bending angle (Table 2) for the orientation and position control algorithms under fixed and moving loading distributions for the beam configurations $[\theta, \phi, L_{SS}]$ and $[\theta, \phi, L_E]$, respectively. As shown in Figure 11a, slacked tendons negatively affect the control accuracy of continuum robot; mean error of 19.77 deg in θ. On the other hand, despite its disadvantages, excessive loading produced more accurate manipulation; mean error of 1.63 deg in θ in Figure 11b. Orientation and position control algorithms under fixed and moving loading distributions decreased the errors down to the range of 3.51 to 4.96 deg. Given the open-loop nature of the testing and evaluation process, the results demonstrate good accuracy and effectiveness for the proposed control algorithms.

For both cases of $[\theta, \phi, L_{SS}]$ and $[\theta, \phi, L_E]$, the errors for orientation control algorithm are similar

This article has been accepted for publication in a future issue of this journal, but has not been fully edited. Content may change prior to final publication. Citation information: DOI 10.1109/ACCESS.2020.3012036, IEEE Access

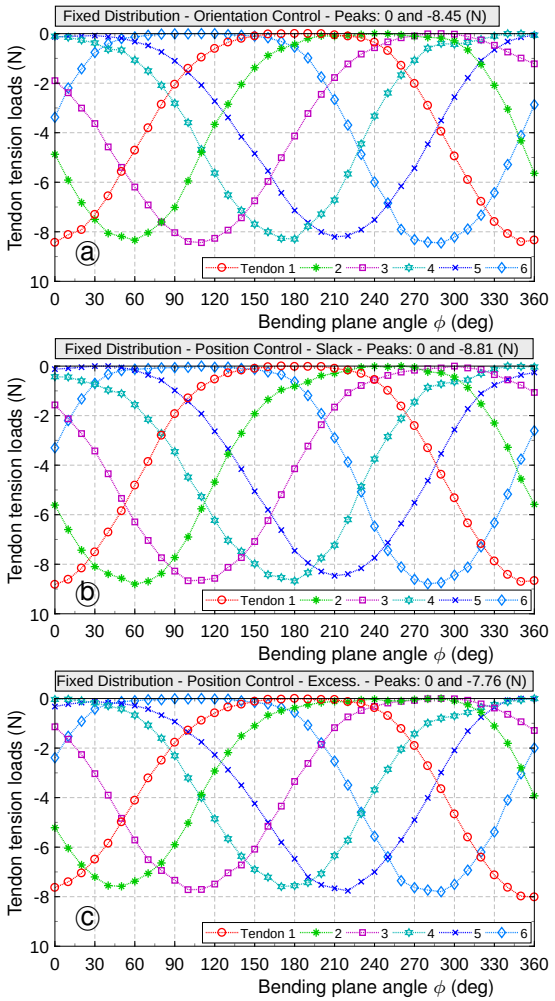

FIGURE 9: Experimental results for the tendon tension loads in a 6-tendon continuum robot for (a) orientation control of beam configurations $[\theta, \phi, L_{SS}]$, (b) position control of beam configurations $[\theta, \phi, L_{SS}]$, and (c) position control of beam configurations $[\theta, \phi, L_E]$ under fixed loading distribution

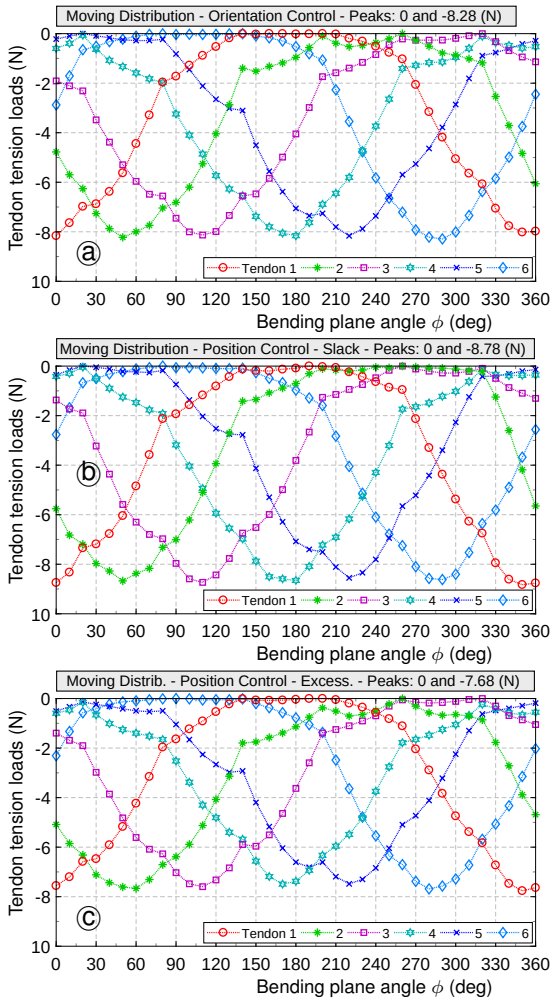

FIGURE 10: Experimental results for the tendon tension loads in a 6-tendon continuum robot for (a) orientation control of beam configurations $[\theta, \phi, L_{SS}]$, (b) position control of beam configurations $[\theta, \phi, L_{SS}]$, and (c) position control of beam configurations $[\theta, \phi, L_E]$ under moving loading distribution

as these algorithms are independent of length. There are no significant differences between the errors for orientation and position control algorithms for any of the cases of slack or excessive loadings. This is because of small differences between the desired θ for both cases of slack and excessive loading (40 deg) and θ_{fp} (40.74 and 39.31 deg) and θ_{mp} (40.6 to 40.74 and 39.18 to 39.31 deg) determined respectively from Equations (15) and (28) for the cases of slack and excessive loading.

To better demonstrate the capability of the algorithms in controlling orientation and position of the continuum structure, a new set of beam configuration is chosen ($[\theta, \phi, L_{AS}]$ - Table 2). This configuration is chosen to produce considerable differences between the given θ and L and those determined from the orientation and position control algorithms. Given the initial length of the continuum structure, commanding the robot to this configuration causes slack in all tendons which results in no movement in the continuum structure. To reach this exact beam configuration, base displacement is required. However, as explained in previous sections, for position control requiring base displacements, a new coor-

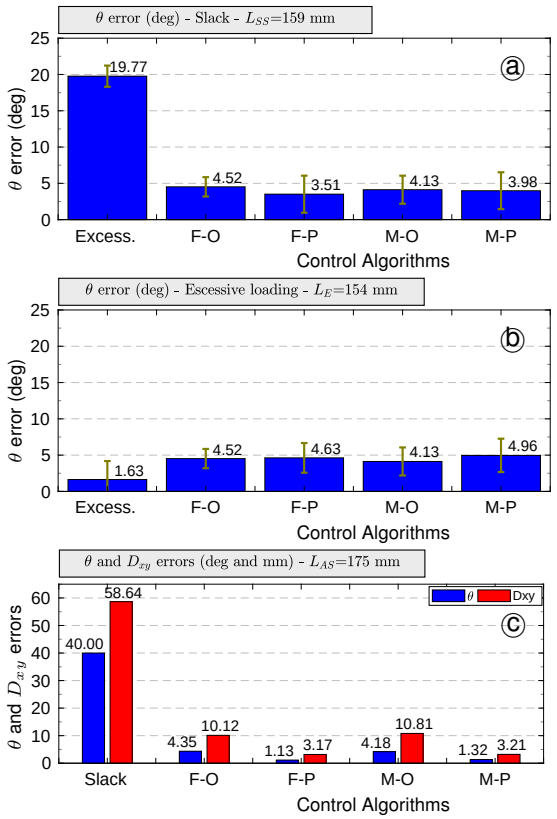

FIGURE 11: Mean and standard deviation of orientation errors for (a) beam configurations $[\theta, \phi, L_{SS}]$, (b) beam configuration $[\theta, \phi, L_E]$ as well as mean orientation and position errors for (c) configurations $[\theta, \phi, L_{AS}]$ for the orientation and position control algorithms under fixed (F-O and F-P) and moving (M-O and M-P) loading distributions in a 6-tendon continuum robot.

dinates is derived to satisfy x and y coordinates of the original target point while the axial displacement of the base compensates for the target z coordinate. Since the experimental setup does not allow base movements, the new point satisfying x and y coordinates is utilized. This is not expected to have any effects on accuracy because the required base movement is a pure straight displacement and does not involve any manipulations in the continuum structure.

The errors in experimental results for bending angle and tip position for the case of traditional inverse kinematics as well as four control algorithms are listed in Figure 11c. Although each algorithm has different target orientation and tip position, the errors are calculated with respect to the original target beam configurations. For the orientation angles, the given θ (40 deg) is used as the reference. The vector sum of x and y coordinates of the tip position (D_{xy} in Figure 4) corresponding to $[\theta, \phi, L_{AS}]$ (58.64 mm) is chosen as the reference for calculating errors in tip positions for different control algorithms. The first column of this figure shows errors as big as the target θ and D_{xy} calculated from the kinematics of the continuum structure for the target configuration. The reason for such big errors is that commanding the actuators displacements calculated using the inverse kinematics for the target configuration ($[\theta, \phi, L_{AS}]$) simply does not cause any movement in the robot at all and only makes all tendons go slack.

As implied from Figures 11c, orientation control algorithms under both fixed and moving loading distributions produced errors as low as 4.35 and 4.18 deg in the bending angle, respectively. Since the objective of these control algorithms is not tip position control, the tip position differences with respect to the given configurations is relatively large; 10.12 and 10.81 mm for fixed and moving loading distributions, respectively. On the other hand, position control algorithms produce small position errors of 3.17 and 3.21 mm under two fixed and moving loading distributions, respectively. The orientation errors of position control algorithms under the two loading distributions (1.13 and 1.32 mm, respectively) listed in this figure are lower than those of the orientation control algorithms. This is because the listed errors are calculated based on the given θ which means the orientation errors for the case of the position control algorithm do not represent the actual orientation error. Computing these errors with respect to the new bending angles calculated by the algorithms (θ_{fp} and θ_{mp} from Equations (15) and (28), respectively produces similar orientation errors as of those in orientation control algorithms for the two loading distributions. These results demonstrates the capability of the proposed control algorithms in controlling orientation and tip position of a continuum robot.

Figure 12 presents the experimental results for the summation of the tension loads in all tendons for each bending plane angle ϕ for orientation control (Figure 12a), position control of beam configuration $[\theta, \phi, L_{SS}]$ (Figure 12b), and $[\theta, \phi, L_E]$ (Figure 12c) under both fixed and moving loading distributions. The experimental results match the simulation results presented in Figure 6 in terms of the magnitude and overall pattern. As implied from these figures, summation of the tension loads for orientation and position control under fixed loading

This article has been accepted for publication in a future issue of this journal, but has not been fully edited. Content may change prior to final publication. Citation information: DOI 10.1109/ACCESS.2020.3012036, IEEE Access

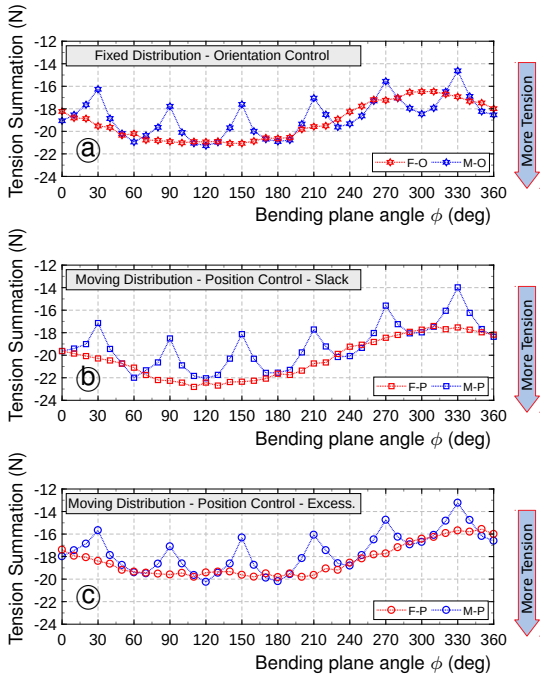

FIGURE 12: Summation of the tension loads in all tendons measured in experiments for (a) orientation control, (b) position control of beam configuration $[\theta, \phi, L_{SS}]$ and (c) $[\theta, \phi, L_E]$ under both fixed and moving loading distributions with respect to the bending plane angle ϕ

distribution are mostly around the maximum absolute values of those of the similar control algorithms under moving loading distribution. In other words, moving loading distribution always produces less tension in tendons than the fixed loading distribution unless the i_m-th tendon is laid on the bending plane ($\alpha_{i_m} - \phi = \pi$) in which case the tensions are equal for both loading distributions.

VII. DISCUSSION

As shown in Figure 12, in a 6-tendon robot, the fixed and moving loading distributions lead to similar tendon tension summations at the bending plane angles of $[0, 60, 120, \ldots, 360]$ deg. Interestingly, the number of maximum peak values (N_{mp}) of the tension summation is directly related to the number of tendons n in the continuum structure. In continuum robots with even number of tendons, the peak values are repeated at the bending plane angles of 0 and 360 deg. However, there is no peak value at the bending plane angle 0 deg in continuum robots with odd number of tendons. This results in no repetition of the peak values in continuum robots with odd number of tendons. It is worth noting that this difference is dependent of the location of the tendons. This relationship is represented as

$$N_{mp} = \begin{cases} n & \text{when } n \text{ is odd} \\ n+1 & \text{when } n \text{ is even} \end{cases} \tag{29}$$

Experimental results validated the numerical simulation and verified the performance of the proposed control algorithms under fixed and moving loading distributions in controlling orientation and position of a 6-tendon continuum robot. The algorithms are proved to be capable of avoiding slack and excessive loading in multi-tendon continuum robots even in open-loop control architecture for a polymer-based continuum manipulator. Based on the application control requirements, e.g. orientation or position control, computational capabilities of the controller, e.g. analytical or numerical iterative solutions, hardware specification, e.g. DOFs and robot workspace, and manipulation features, e.g. motion smoothness, the proposed control algorithms may be chosen to manipulate a continuum robot with any number of tendons without concern about slack deficiencies or excessive loading damage.

Stiffness of a continuum structure may be controlled by manipulating the tension loads in tendons. Reduction of the stiffness of the continuum robot can enable safe navigation inside delicate confined spaces, e.g. to avoid wall puncture. In contrast, a high stiffness continuum structure may be advantageous during tissue manipulation [14], [38], [39]. In order to avoid both slack and unnecessary loading in tendons and also to adjust stiffness in the continuum structure, the location of the zero-load axis can be moved behind virtual tendon so that there is a minimum tension loading of F_0 in the virtual tendon. The minimum tension loading F_0 in tendons may be used to trade off between tension loading magnitudes and beam manipulator stiffness required for any applications. Changing F_0 directly affects the stiffness of the manipulator. The larger F_0 values, the stiffer manipulator. The minimum allowable value of F_0 is zero and negative values cause slack in some or all of the tendons.

VIII. CONCLUSION

In this work, orientation and position control algorithms developed based on two fixed and moving loading distributions in n-tendon continuum robots. These loading distributions were designed to prevent slack and excessive loading in tendons. The algorithms were developed to account for the bending and axial compliance of the continuum structure as well as tendon compliance. Numerical

simulations were performed to help describe the control algorithms and their key characteristic features under fixed and moving loading distributions. The effectiveness of the proposed control algorithms in avoiding slack and excessive loadings in tendons and controlling the orientation and tip position of the continuum structure for different beam configurations was experimentally verified using a 6-tendon continuum robotic system in open-loop control architecture. Future works may take friction and external loading and disturbance into consideration and address experimental characterization of off-the-shelf catheters and continuum robots.

REFERENCES

[1] R. Cieslak and A. Morecki, "Elephant trunk type elastic manipulator-a tool for bulk and liquid materials transportation," *Robotica*, vol. 17, no. 01, pp. 11–16, 1999.

[2] I. D. Walker, D. M. Dawson, T. Flash, F. W. Grasso, R. T. Hanlon, B. Hochner, W. M. Kier, C. C. Pagano, C. D. Rahn, and Q. M. Zhang, "Continuum robot arms inspired by cephalopods," in *Defense and Security*. International Society for Optics and Photonics, 2005, pp. 303–314.

[3] C. B. Cay and B. A long handled, "The functional morphology of the musculature of squid (Loliginidae) arms and tentacles," *Journal of Morphology*, vol. 172, pp. 179–192, 1982.

[4] M. Tanaka and K. Tanaka, "Control of a snake robot for ascending and descending steps," *Robotics, IEEE Transactions on*, vol. 31, no. 2, pp. 511–520, 2015.

[5] A. M. Andruska and K. S. Peterson, "Control of a snake-like robot in an elastically deformable channel," *Mechatronics, IEEE/ASME Transactions on*, vol. 13, no. 2, pp. 219–227, 2008.

[6] M. A. Armada, G. Granosik, M. G. Hansen, and J. Borenstein, "The OmniTread serpentine robot for industrial inspection and surveillance," *Industrial Robot: An International Journal*, vol. 32, no. 2, pp. 139–148, 2005.

[7] A. Wolf, H. B. Brown, R. Casciola, A. Costa, M. Schwerin, E. Shamas, and H. Choset, "A mobile hyper redundant mechanism for search and rescue tasks," in *Intelligent Robots and Systems, 2003.(IROS 2003). Proceedings. 2003 IEEE/RSJ International Conference on*, vol. 3. IEEE, 2003, pp. 2889–2895.

[8] H. B. Gilbert, J. Neimat, and R. J. Webster, "Concentric tube robots as steerable needles: achieving follow-the-leader deployment," *Robotics, IEEE Transactions on*, vol. 31, no. 2, pp. 246–258, 2015.

[9] N. Simaan, K. Xu, W. Wei, A. Kapoor, P. Kazanzides, R. Taylor, and P. Flint, "Design and integration of a telerobotic system for minimally invasive surgery of the throat," *The International Journal of Robotics Research*, vol. 28, no. 9, pp. 1134–1153, 2009.

[10] B. A. Jones and I. D. Walker, "Kinematics for multisection continuum robots," *Robotics, IEEE Transactions on*, vol. 22, no. 1, pp. 43–55, 2006.

[11] Y.-J. Kim, S. Cheng, S. Kim, and K. Iagnemma, "A novel layer jamming mechanism with tunable stiffness capability for minimally invasive surgery," *Robotics, IEEE Transactions on*, vol. 29, no. 4, pp. 1031–1042, 2013.

[12] C. Bergeles, A. H. Gosline, N. V. Vasilyev, P. J. Codd, P. J. del Nido, and P. E. Dupont, "Concentric tube robot design and optimization based on task and anatomical constraints," *Robotics, IEEE Transactions on*, vol. 31, no. 1, pp. 67–84, 2015.

[13] Y.-J. Kim, S. Cheng, S. Kim, and K. Iagnemma, "A stiffness-adjustable hyperredundant manipulator using a variable neutral-line mechanism for minimally invasive surgery," *Robotics, IEEE Transactions on*, vol. 30, no. 2, pp. 382–395, 2014.

[14] I. D. Walker, "Continuous backbone "continuum" robot manipulators," *ISRN Robotics*, vol. 2013, 2013.

[15] R. J. Webster and B. A. Jones, "Design and kinematic modeling of constant curvature continuum robots: A review," *The International Journal of Robotics Research*, 2010.

[16] A. Muller, "Internal preload control of redundantly actuated parallel manipulators-its application to backlash avoiding control," *IEEE Transactions on Robotics*, vol. 21, no. 4, pp. 668–677, 2005.

[17] D. B. Camarillo, C. F. Milne, C. R. Carlson, M. R. Zinn, and J. K. Salisbury, "Mechanics modeling of tendon-driven continuum manipulators," *Robotics, IEEE Transactions on*, vol. 24, no. 6, pp. 1262–1273, 2008.

[18] A. Trevisani, "Planning of dynamically feasible trajectories for translational, planar, and underconstrained cable-driven robots," *Journal of Systems Science and Complexity*, vol. 26, no. 5, pp. 695–717, 2013.

[19] Y. Chen, J. H. Chang, A. S. Greenlee, K. C. Cheung, A. H. Slocum, and R. Gupta, "Multi-turn, tension-stiffening catheter navigation system," in *Robotics and Automation (ICRA), 2010 IEEE International Conference on*. IEEE, 2010, pp. 5570–5575.

[20] M. Gouttefarde, J. Lamaury, C. Reichert, and T. Bruckmann, "A versatile tension distribution algorithm for n-DOF parallel robots driven by n+ 2 cables," *IEEE Transactions on Robotics*, vol. 31, no. 6, pp. 1444–1457, 2015.

[21] R. L. Williams, P. Gallina, and J. Vadia, "Planar translational cable-direct-driven robots," *Journal of Field Robotics*, vol. 20, no. 3, pp. 107–120, 2003.

[22] M. Carricato and J.-P. Merlet, "Stability analysis of underconstrained cable-driven parallel robots," *IEEE Transactions on Robotics*, vol. 29, no. 1, pp. 288–296, 2013.

[23] S. Fang, D. Franitza, M. Torlo, F. Bekes, and M. Hiller, "Motion control of a tendon-based parallel manipulator using optimal tension distribution," *Mechatronics, IEEE/ASME Transactions on*, vol. 9, no. 3, pp. 561–568, 2004.

[24] P. H. Borgstrom, B. L. Jordan, G. S. Sukhatme, M. A. Batalin, and W. J. Kaiser, "Rapid computation of optimally safe tension distributions for parallel cable-driven robots," *IEEE Transactions on Robotics*, vol. 25, no. 6, pp. 1271–1281, 2009.

[25] M. C. Yip, J. A. Sganga, and D. B. Camarillo, "Autonomous control of continuum robot manipulators for complex cardiac ablation tasks," *Journal of Medical Robotics Research*, vol. 2, no. 01, p. 1750002, 2017.

[26] D. B. Camarillo, C. R. Carlson, and J. K. Salisbury, "Configuration tracking for continuum manipulators with coupled tendon drive," *Robotics, IEEE Transactions on*, vol. 25, no. 4, pp. 798–808, 2009.

[27] M. Haghighipanah, M. Miyasaka, and B. Hannaford, "Utilizing elasticity of cable-driven surgical robot to estimate cable tension and external force," *IEEE Robotics and Automation Letters*, vol. 2, no. 3, pp. 1593–1600, 2017.

[28] T. Kato, I. Okumura, S.-E. Song, A. J. Golby, and N. Hata, "Tendon-driven continuum robot for endoscopic surgery: Preclinical development and validation of a tension propagation model," *IEEE/ASME Transactions on Mechatronics*, vol. 20, no. 5, pp. 2252–2263, 2015.

[29] B. L. Conrad and M. R. Zinn, "Interleaved continuum-rigid manipulation: an approach to increase the capability of minimally invasive surgical systems," *IEEE/ASME Transactions on Mechatronics*, vol. 22, no. 1, pp. 29–40, 2017.

[30] M. Khoshnam and R. V. Patel, "Tendon-sheath analysis for modeling and control of steerable ablation catheters," in *Advanced Intelligent Mechatronics (AIM), 2016 IEEE International Conference on*. IEEE, 2016, pp. 1585–1590.

[31] E. Naerum, H. H. I. King, and B. Hannaford, "Robustness of the unscented kalman filter for state and parameter estimation

in an elastic transmission." in *Robotics: Science and Systems*, 2009.

[32] S. N. Kosari, S. Ramadurai, H. J. Chizeck, and B. Hannaford, "Control and tension estimation of a cable driven mechanism under different tensions," in *ASME 2013 International Design Engineering Technical Conferences and Computers and Information in Engineering Conference*. American Society of Mechanical Engineers, 2013, pp. V06AT07A077—-V06AT07A077.

[33] R. Roy, L. Wang, and N. Simaan, "Modeling and estimation of friction, extension, and coupling effects in multisegment continuum robots," *IEEE/ASME Transactions on Mechatronics*, vol. 22, no. 2, pp. 909–920, 2017.

[34] M. M. Dalvand, S. Nahavandi, and R. D. Howe, "An analytical loading model for n-tendon continuum robots," *IEEE Transactions on Robotics*, pp. 1–11, 2018.

[35] P. M. Loschak, L. J. Brattain, and R. D. Howe, "Automated pointing of cardiac imaging catheters," in *Robotics and Automation (ICRA), 2013 IEEE International Conference on*. IEEE, 2013, pp. 5794–5799.

[36] B. He, Z. Wang, Q. Li, H. Xie, and R. Shen, "An analytic method for the kinematics and dynamics of a multiple-backbone continuum robot," *Int J Adv Robotic Sy*, vol. 10, no. 84, 2013.

[37] M. Moradi Dalvand, S. Nahavandi, and R. D. Howe, "Fast vision-based catheter 3D reconstruction." *Physics in medicine and biology*, vol. 61, no. 14, pp. 5128– 5148, 2016.

[38] M. Mahvash and P. E. Dupont, "Stiffness control of surgical continuum manipulators," *IEEE Transactions on Robotics*, vol. 27, no. 2, pp. 334–345, 2011.

[39] ——, "Stiffness control of a continuum manipulator in contact with a soft environment," in *Intelligent Robots and Systems (IROS), 2010 IEEE/RSJ International Conference on*. IEEE, 2010, pp. 863–870.